JBC ARTICLE

Role of a conserved glutamine in the function of voltage-gated Ca^{2+} channels revealed by a mutation in human *CACNA1D*

Received for publication, April 24, 2018, and in revised form, July 24, 2018 Published, Papers in Press, July 27, 2018, DOI 10.1074/jbc.RA118.003681

Edgar Garza-Lopez[‡], Josue A. Lopez[‡], Jussara Hagen[‡], Ruth Sheffer[§], Vardiella Meiner[§], and Amy Lee[‡1]

From the [‡]Departments of Molecular Physiology and Biophysics, Otolaryngology Head-Neck Surgery, and Neurology and Iowa Neuroscience Institute, University of Iowa, Iowa City, Iowa 52242 and [§]Department of Genetics and Metabolic Diseases, Hadassah-Hebrew University Medical Center, Jerusalem 91120, Israel

Edited by Mike Shipston

Voltage-gated Ca_v Ca^{2+} channels play crucial roles in regulating gene transcription, neuronal excitability, and synaptic transmission. Natural or pathological variations in Ca_v channels have yielded rich insights into the molecular determinants controlling channel function. Here, we report the consequences of a natural, putatively disease-associated mutation in the *CACNA1D* gene encoding the pore-forming $Ca_v1.3$ α_1 subunit. The mutation causes a substitution of a glutamine residue that is highly conserved in the extracellular S1–S2 loop of domain II in all Ca_v channels with a histidine and was identified by whole-exome sequencing of an individual with moderate hearing impairment, developmental delay, and epilepsy. When introduced into the rat $Ca_v1.3$ cDNA, Q558H significantly decreased the density of Ca^{2+} currents in transfected HEK293T cells. Gating current analyses and cell-surface biotinylation experiments suggested that the smaller current amplitudes caused by Q558H were because of decreased numbers of functional $Ca_v1.3$ channels at the cell surface. The substitution also produced more sustained Ca^{2+} currents by weakening voltage-dependent inactivation. When inserted into the corresponding locus of $Ca_v2.1$, the substitution had similar effects as in $Ca_v1.3$. However, the substitution introduced in $Ca_v3.1$ reduced current density, but had no effects on voltage-dependent inactivation. Our results reveal a critical extracellular determinant of current density for all Ca_v family members and of voltage-dependent inactivation of $Ca_v1.3$ and $Ca_v2.1$ channels.

Within the human genome, hundreds of genes encode ion channels, mutations which cause diseases affecting a variety of organ systems (1). In many cases, electrophysiological analysis of the mutations has uncovered mechanistic insights into channel function. Mutations causing long QT syndrome have revealed molecular determinants controlling voltage-dependent activation (2) and inactivation (3). In addition, the functional characterization of a mutation causing congenital stationary night blindness in the *CACNA1F* gene encoding voltage-gated $Ca_v1.4$ Ca^{2+} channels uncovered a role for a C-terminal automodulatory domain that suppresses Ca^{2+}-dependent inactivation of these channels (4). Thus, the study of channelopathy-causing mutations can advance understanding of the structure–function relationships of ion channel proteins as well as inform about the physiological roles of these channels in humans.

In addition to congenital stationary night blindness, mutations affecting voltage-gated Ca^{2+} channels cause migraine, ataxia, malignant hypothermia, and cardiac arrhythmia (5, 6). Within the Ca_v channel[2] superfamily, $Ca_v1.3$ L-type channels have emerged as targets of heterogeneous disorders including deafness and autism (7, 8). In the ear, $Ca_v1.3$ channels are localized at inner hair cell synapses where they mediate Ca^{2+} influx required for transmission of auditory information into the brain via the auditory nerve (9, 10). A mutation involving a glycine insertion in the domain IS6 transmembrane helix prevents voltage-dependent gating of $Ca_v1.3$ channels and causes deafness in homozygous individuals carrying this mutation (11). $Ca_v1.3$ channels are also expressed in the brain, where they regulate mood-related behaviors (12) and fear consolidation (13). *De novo* mutations causing a gain of function in $Ca_v1.3$ are associated with intellectual disability and autism spectrum disorders (7, 8).

Here, we report the functional effects of a mutation in the *CACNA1D* gene encoding $Ca_v1.3$ found by exome sequencing of an individual with intellectual disability, developmental delay, and mild hearing impairment. We show that this mutation, which causes a histidine substitution for a glutamine residue in the extracellular loop connecting the S1 and S2 helices in domain II (IIS1–S2L), causes a significant reduction in $Ca_v1.3$ current density and yet suppresses voltage-dependent inactivation of these channels in transfected cells. The glutamine residue is conserved in all Ca_v family members and its mutation to histidine has similar effects when introduced into

This work was supported by Karl Kahane Foundation (to V. M. and R. S.), Conacyt (Mexico) postdoctoral fellowship (to E. G. L.), and National Institutes of Health Grants NS084190 and DC009433 and Carver Research Program of Excellence Award (to A. L.). The authors declare that they have no conflicts of interest with the contents of this article. The content is solely the responsibility of the authors and does not necessarily represent the official views of the National Institutes of Health.

[1] To whom correspondence should be addressed: PBDB 5318, 169 Newton RD, Iowa City, IA 52242. Tel.: 319-384-1762; Fax: 319-335-7330; E-mail: amy-lee@uiowa.edu.

[2] The abbreviations used are: Ca_v channel, voltage-gated calcium channel; I-V, current-voltage; a.u., arbitrary unit; ANOVA, analysis of variance; VDI, voltage-dependent inactivation; VSD, voltage sensor domain; ASD, autism spectrum disorder; fC; femtocoulomb.

$Ca_v2.1$ and $Ca_v3.1$ channels. Our findings implicate IIS1–S2L as a key determinant for regulating the cell-surface density and inactivation gating of Ca_v channels.

Results

Q567H mutation in an individual with moderate hearing impairment and intellectual disability

The male proband was the first-born child of healthy parents who were first cousins of Arabic descent. The father had a history of febrile seizures since childhood. The proband was born after an uneventful pregnancy and delivered at 38 weeks of gestation by cesarean section because of fetal distress. He failed the hearing test at birth and had seizures beginning at 4 months of age. At the age of 4 ½ years, he was reassessed at the genetic clinic for the purpose of family planning. He did not speak and his comprehension was limited. He exhibited autistic behaviors including very limited eye contact and hyperactivity. He wore hearing aids from the age of 11 months. At 5 years of age, he underwent hearing tests which revealed moderate hearing loss (40–50 db SPL across all frequencies from 500 Hz to 40 kHz).

Whole-exome sequencing and filtering for homozygous variants revealed two potential candidate genes: A homozygous mutation in the otogelin gene (*OTOG*): Chr11(GRCh37): g.17631250C>T; NM_001277269.1: c.4439C>T (p.Thr1480Ile); and a homozygous missense variant in *CACNA1D*: Chr3 (GRCh37): g.53756476G>C; NM_000720.3: c.1701G>C (p.Gln567His). The *OTOG* variant was present in a heterozygous state in the gnomAD browser (0.00003348), whereas the *CACNA1D* was found neither in gnomAD nor in an in-house exome database. Both parents were heterozygous for the *OTOG* and *CACNA1D* variants. The high degree of consanguinity within the family was the basis for assuming a recessive model of inheritance. A full pedigree molecular analysis was not possible because of difficulties in obtaining consent from other family members.

OTOG encodes otogelin, an *N*-glycosylated protein that is enriched in cellular membranes of the inner ear (14). Mutations in *OTOG* cause autosomal-recessive moderate hearing impairment (15). *CACNA1D* encodes the pore-forming subunit of $Ca_v1.3$ Ca^{2+} channels (Fig. 1*A*), which mediate the presynaptic release of glutamate from inner hair cells in the cochlea (9, 16). A mutation in *CACNA1D* that causes a complete loss of $Ca_v1.3$ function causes congenital deafness and sinoatrial node dysfunction (11). *CACNA1D* variants have also been associated with autism spectrum disorders (8) and epilepsy (8, 17, 18). Because of the coincident involvement of *CACNA1D* in the proband's symptoms (*i.e.* hearing loss, epilepsy, autism), we analyzed the functional consequences of the *CACNA1D* in a heterologous expression system.

The Gln to His mutation decreases current density and cell-surface levels of $Ca_v1.3$

The mutation in the affected individual causes substitution of a histidine for a glutamine residue in the proximal third of the extracellular loop connecting transmembrane helices S1 and S2 in domain II (Q567H) (Fig. 1*B*). To elucidate the functional consequences of Q567H, we introduced this mutation in the corresponding region of the rat $Ca_v1.3$ channel (Q558H). We

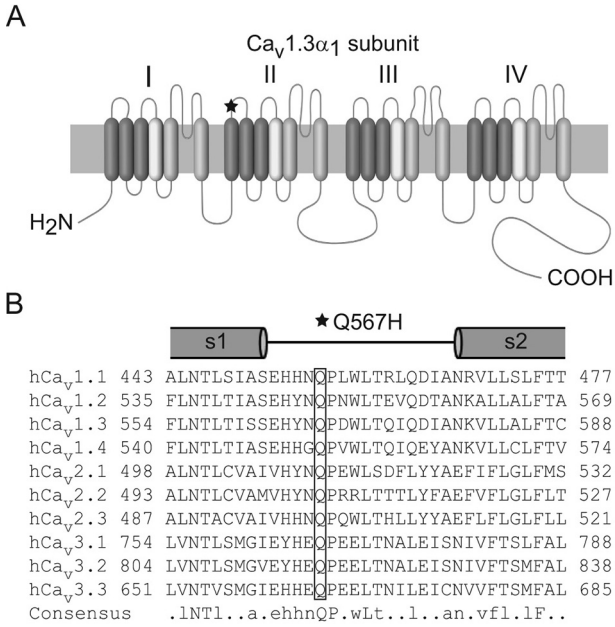

Figure 1. Q567H is located in the extracellular S1–S2 loop of domain II in the $Ca_V1.3$ α_1 subunit. *A*, schematic of $Ca_V1.3$ α_1 subunit with the mutation indicated (*star*). *B*, alignment of amino acids corresponding to this extracellular loop flanked by portions of S1 and S2. *Box* indicates conserved glutamine that is substituted with histidine because of the mutation. *Capital letters* indicate amino acids that are conserved in all sequences. *Lowercase letters* indicate conserved amino acids in at least six sequences.

used whole-cell patch clamp electrophysiology to compare the properties of the wild-type (WT) and mutant channels coexpressed with the auxiliary β_{2a} and $\alpha_2\delta_1$ subunits in human embryonic kidney cells transformed with T-antigen (HEK293T). In current-voltage (I-V) relationships, the most prominent difference between cells transfected with WT and Q558H was a significant reduction in the peak current density of the mutant channel as compared with the WT channel (Fig. 2*A*; Table 1). To determine whether this was because of alterations in the number of functional Q558H channels and/or their open probability, we analyzed gating currents evoked by depolarization to the reversal potential (I_{gating}) and tail currents (I_{tail}) upon repolarization to the holding voltage (Fig. 2*B*). As was described previously (19, 20), the time integral of I_{gating} (Q_{max}) is a measure of the number of channels in the cell membrane, and the ratio of I_{tail} and Q_{max} describes the relative channel open probability. Q558H caused a significant reduction in Q_{max} (56.5 ± 6.4 fC for WT *versus* 16 ± 2.1 fC for Q558H; $p < 0.01$ by *t* test), but no change in the slope of the I_{tail} *versus* Q_{max} relationship (9.8 ± 0.8 for WT *versus* 12.4 ± 1.2 for Q558H; $p = 0.62$ by F-test) (Fig. 2*C*). Thus, Q558H causes a decrease in the number of functional channels, but not their open probability.

Q558H could cause greater degradation of the channel because of improper folding. Alternatively, the mutation could alter the trafficking of the channel to or from the plasma membrane. To distinguish between these possibilities, we compared the amount of plasma membrane–associated WT and mutant channel protein in cell-surface biotinylation assays. Cell-surface proteins were subject to biotinylation and pulldown by streptavidin beads, and the levels of WT and mutant channels were compared by Western blotting with $Ca_v1.3$ antibodies.

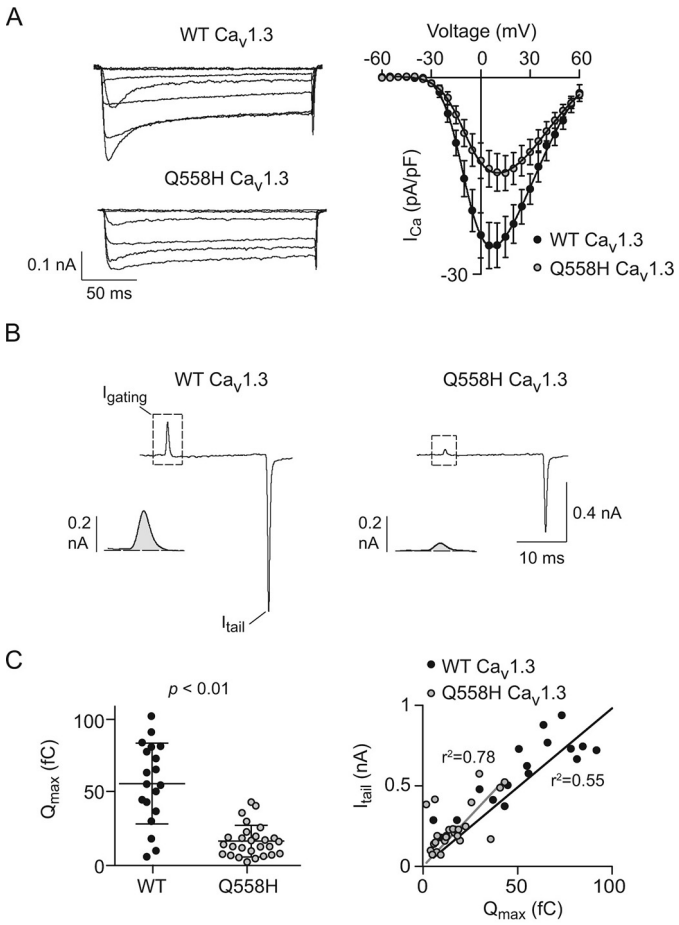

Figure 2. Q558H reduces current density and the number of functional $Ca_v1.3$ channels. *A*, *left*, family of representative current traces obtained using 200-ms test pulses to various voltages from a holding voltage of −80 mV. *Right*, current-voltage (I-V) plots. *n* values and I-V parameters are listed in Table 1. Results are from four independent experiments. *B*, representative traces showing I_{gating} evoked by a 20-ms step depolarization from −80 mV to +70 mV and I_{tail} upon repolarization to −80 mV. *Insets* show I_{gating} and I_{tail} on expanded time scale. *C*, *left*, average maximal gating charge (Q_{max}) for WT and mutant; *p* value was determined by *t* test. *Right*, I_{tail} for each cell is plotted against Q_{max}. The fit by linear regression and coefficient of determination (r^2) are shown for WT ($n = 19$ cells) and Q558H ($n = 27$ cells). Results are from four independent experiments. *Error bars* represent S.E.

Table 1

Parameters of I-V relationships

Values for $V_{½}$ and *k* were obtained from Boltzmann fits of data in Fig. 2*A*. Results were obtained from six independent experiments, and *p* values were determined by *t* test. pA/pF, picoamperes/picofarads.

Channel	WT	*n*	Mutant	*n*	*p* value
$Ca_V1.3$					
$V_{½}$ (mV)	−9.9 ± 1.4	10	−6.8 ± 1.2	11	0.12
k	7.1 ± 0.5		10.2 ± 1.2		0.03
I_{Ca} density (pA/pF)	−25.6 ± 3.3		−14.5 ± 2.8		0.02
$Ca_V2.1$					
$V_{½}$ (mV)	−2.4 ± 1.1	8	0.7 ± 1.4	9	0.11
k	3.1 ± 0.5		3.6 ± 0.5		0.51
I_{Ca} density (pA/pF)	−72.8 ± 12		−30.1 ± 7.8		0.03
$Ca_V3.1$					
$V_{½}$ (mV)	−41.8 ± 1.2	11	−40.7 ± 0.8	14	0.43
k	3.3 ± 0.4		3.4 ± 0.4		0.83
I_{Ca} density (pA/pF)	−165.5 ± 14		−67.9 ± 13		<0.01

Blotting with antibodies of Na^+/K^+ ATPase was used as a positive control for the cell-surface biotinylation reaction. Expression of the WT or mutant channels had no effect on

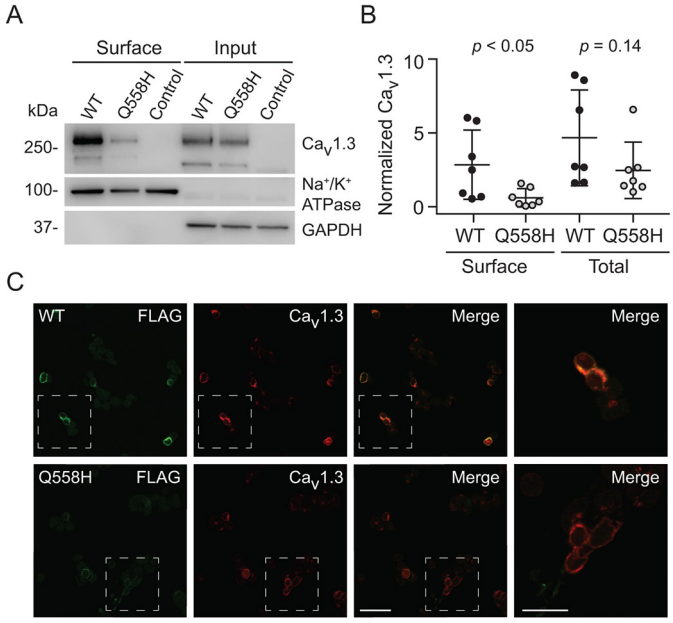

Figure 3. Q558H reduces the cell-surface density of $Ca_v1.3$. *A*, Western blotting of lysates of untransfected HEK293T cells (*Control*) or cells transfected with β_{2a}, $\alpha_2\delta_1$, and WT Cav1.3 or Q567H mutant channels. Blots were probed with $Ca_v1.3$ antibodies showing levels of total (*Input*) or surface protein isolated by exposing transfected cells to biotinylation reagents prior to lysis and pulldown on Neutravidin beads. Blots were also probed with antibodies against Na^+/K^+ ATPase and GAPDH as normalization controls. *B*, densitometric analysis of total and surface $Ca_v1.3$ protein. From Western blots obtained as in *A*, signals corresponding to surface $Ca_v1.3$ protein were normalized to those for Na^+/K^+ ATPase (*Surface*), and the signals for total $Ca_v1.3$ protein were normalized to those for GAPDH. Results are from seven independent experiments. *Error bars* represent S.E. *C*, representative confocal images from HEK293T cells transfected with β_{2a}, $\alpha_2\delta_1$, and WT FLAG-$Ca_v1.3$ (*top*) or FLAG-Q558H mutant channels (*bottom*) labeled under nonpermeabilized conditions with FLAG antibodies to mark cell-surface channels (*green*), and following detergent permeabilization, with $Ca_v1.3$ antibodies to label the total population of intracellular and cell-surface channels (*red*). The degree of cell-surface labeling is indicated by regions of overlap of the *red* and *green* channels (*yellow*, *Merge*). *Boxed region* is shown at higher magnification in far *left panel*, and indicates weaker cell-surface labeling of the mutant compared with WT channel. *Scale bars*: 20 μm in *initial three panels*, 10 μm in *far right panel*. Results are representative of two independent experiments.

the amount of cell-surface Na^+/K^+ ATPase as the corresponding signals measured by densitometry were not significantly different in untransfected control cells (0.28 ± 0.1 arbitrary units (a.u.)) or those transfected with WT (0.33 ± 0.11 a.u.) or Q558H (0.24 ± 0.07 a.u.; $p = 0.83$ by analysis of variance (ANOVA)).

Although there was no difference in the total levels of WT and mutant channel protein in whole-cell lysates, there was a significant reduction in the levels of Q558H channel protein at the cell surface compared with WT channels (Fig. 3, *A* and *B*). To confirm these results, we also compared the cell-surface localization of WT and Q558H mutant channels containing an extracellular FLAG epitope between S5 and S6 of domain II. Consistent with the lack of effect of epitopes in this region on channel function (21), these FLAG-tagged channels exhibited similar electrophysiological properties as the untagged channels (data not shown). Cells transfected with FLAG-tagged WT and mutant channels were labeled first with FLAG antibodies under nonpermeabilizing conditions followed by permeabilization and labeling with $Ca_v1.3$ antibodies to mark the distribution of cell-surface and total channels, respectively. Because of

our transient transfection strategy, channel expression levels varied considerably between cells as detected by $Ca_v1.3$ immunofluorescence, and this impacted the intensity of cell-surface FLAG-labeled channels. However, in cells selected for a similar level of total $Ca_v1.3$ labeling, FLAG labeling was less apparent at the plasma membrane when transfected with Q558H than with the WT channel (Fig. 3*C*). Taken together, our results show that Q558H causes a loss of function because of improper cell-surface trafficking of $Ca_v1.3$.

Q558H alters voltage-dependent inactivation of $Ca_v1.3$

Compared with WT currents, Ca^{2+} currents (I_{Ca}) mediated by Q558H channels were more prolonged (Fig. 2*A*), suggesting defects in inactivation kinetics. To characterize this more thoroughly, we performed exponential curve fitting of I_{Ca} evoked by sustained (3-s) pulses to +10 mV from a holding voltage of −80 mV. Traces corresponding to WT and mutant I_{Ca} were best fit with a double-exponential function, indicating the presence of a fast and slow phase of inactivation. Compared with WT channels, the time constant (τ_{fast}) and fractional amplitude of the fast phase of inactivation (F_{fast}) were significantly reduced in mutant channels (Fig. 4, *A–C*). Conversely, the time constant (τ_{slow}) and fractional amplitude of slow inactivation (F_{slow}) for the mutant channels were significantly greater than for WT channels (Fig. 4, *A–C*). These results indicate that Q558H prolongs $Ca_v1.3$ currents by stabilizing slow inactivation.

To investigate effects of Q558H on the voltage-dependence of inactivation, we measured the impact of a 5-s conditioning prepulse to various voltages on inactivation of a test current evoked by a 40-ms pulse to +10 mV. The amplitude of the test current was normalized to that with a −60 mV prepulse (Normalized I_{Ca}) and plotted against prepulse voltage. Note that although we used Ca^{2+} as the charge carrier, this voltage protocol measures voltage-dependent inactivation (VDI) rather than Ca^{2+}-dependent inactivation given the relatively long duration of the conditioning prepulse (22). Consistent with a voltage-dependent process, Boltzmann fits of the data showed a sigmoidal dependence on prepulse voltage. Parameters from these fits indicated no difference in the voltage of half-maximal inactivation ($V_{½}$) but a significantly greater slope (k) for Q558H compared with WT channels (Fig. 5*A*; Table 2). To determine whether this effect of Q558H might be secondary to effects on voltage-dependent activation, we analyzed the amplitude of tail currents measured by 2-ms repolarizations to −60 mV from various test voltages. The amplitudes of tail currents were normalized to that using a +40 mV test pulse and plotted against test voltage. Boltzmann fits of the data yielded similar parameters for WT and Q558H channels in terms of V_h and k (Fig. 5*B*; Table 3), which argued against an effect of Q558H on voltage-dependent activation. Overlay of the inactivation and activation curves revealed a sizeable increase in window currents generated by Q558H (Fig. 5*C*). Thus, despite the decrease in peak current density caused by Q558H, the mutation also has a gain of function effect in allowing Ca^{2+} entry at voltages at which WT channels are inactivated.

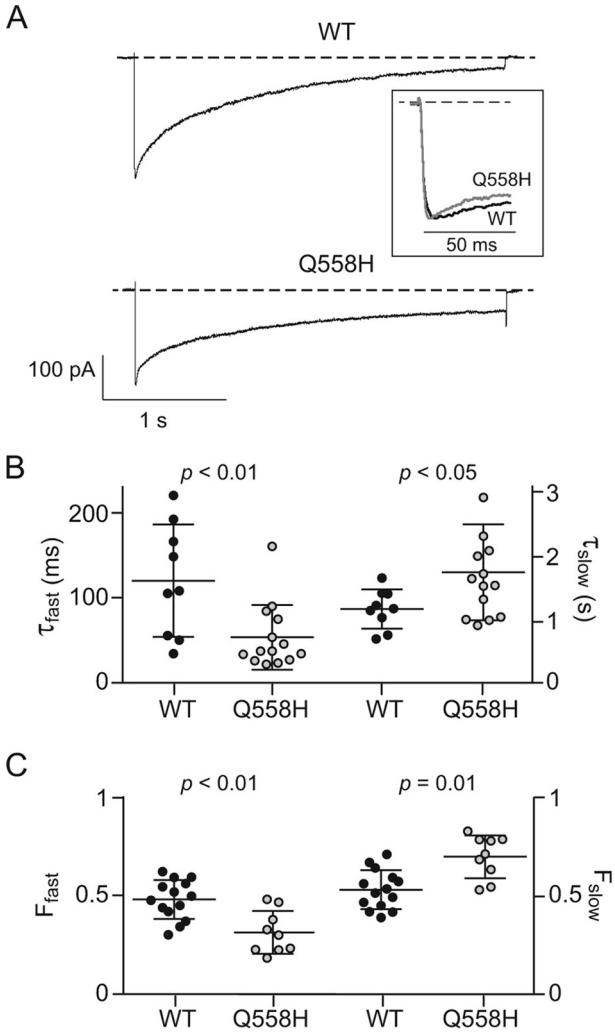

Figure 4. Q558H modifies inactivation of $Ca_v1.3$ during sustained depolarizations. *A*, representative traces for currents evoked by a 3-s test pulse from −80 mV to +10 mV in cells transfected with WT or mutant channels. *Inset*, normalized traces of the displayed currents with expanded time scale showing faster initial inactivation of Q558H compared with WT. *B* and *C*, comparison of kinetics of inactivation of WT ($n = 9$ cells) and Q558H channels ($n = 14$ cells). Time constants (τ_{fast}, τ_{slow}) (*B*) and fractional amplitudes (F_{fast} and F_{slow}) (*C*) were obtained from double exponential fits of current traces obtained as in (*A*). *Error bars* represent S.E. *p* values were determined by *t* test. Results are from five independent experiments.

Alterations in $Ca_v2.1$ and $Ca_v3.1$ properties by similar Gln to His mutations

The strong conservation of Gln-567 (Fig. 1*B*) suggests that it may play a key role in regulating current density and steady-state inactivation of all Ca_v channel family members. To test this, we introduced the Gln to His mutation in the corresponding sites of $Ca_v2.1$ (Q511H) and the more distantly related $Ca_v3.1$ (Q767H). Similar to the effects of Q558H in $Ca_v1.3$ (Fig. 2), Q511H and Q767H caused significant reductions in peak current densities but without a change in Boltzmann parameters for the I-V relationship (Fig. 6, *A* and *B*; Table 1). We were unable to test whether the reduced peak current density for Q511H and Q767H was due to decreased cell-surface channel protein, as was done for $Ca_v1.3$ and Q567H (Fig. 3, *A* and *B*) because of low levels of cell-surface biotinylation of the mutant channels. However, gating current analyses revealed a signifi-

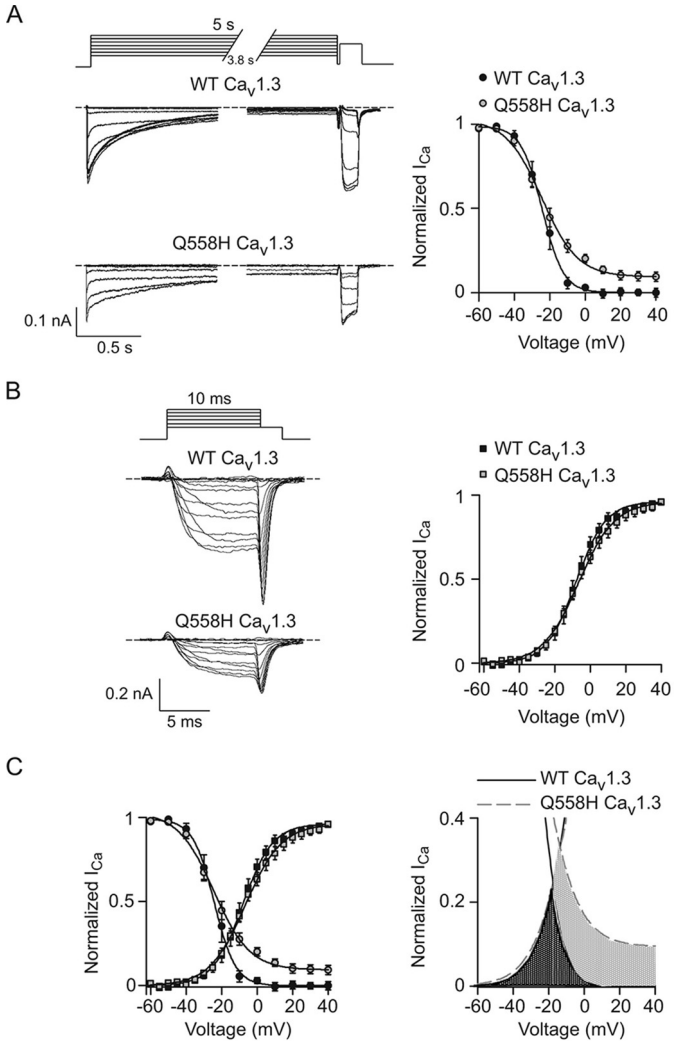

Figure 5. Q558H suppresses voltage-dependent inactivation of $Ca_v1.3$. *A*, *left*, representative traces of currents evoked by 5-s prepulses to various voltages prior to a 40-ms test pulse to +10 mV from a holding voltage of −80 mV. *Right*, test current amplitudes were normalized with the test current amplitude obtained to −60 mV and plotted against prepulse voltage for WT ($n = 7$ cells) and Q558H mutant channels ($n = 7$ cells). *B*, *left*, representative traces of currents evoked by 10-ms steps to various voltages prior to 2-ms repolarization to −60 mV to better resolve tail currents. The amplitudes of tail currents were normalized to those obtained with +40 mV test pulse and plotted against test voltage for WT ($n = 9$ cells) and Q558H mutant channels ($n = 10$ cells). *C*, *left*, overlay of activation and inactivation curves for WT and mutant channels from data in *A* and *B*. *Right*, data from *C* are shown on expanded vertical scale. Window current of Q558H (*gray shading*) extends to depolarized voltages at which WT window current (*dark shading*) is absent. Results are from six independent experiments. *Error bars* represent S.E.

Table 2

Parameters for voltage-dependent inactivation

Values for $V_{½}$ and k were obtained from Boltzmann fits of data in Fig. 5*A*. Results were obtained from nine independent experiments, and p values were determined by t test.

Channel	WT	*n*	Mutant	*n*	*p* value
$Ca_V1.3$					
$V_{½}$ (mV)	−24.6 ± 2.1	7	−21.5 ± 1.9	7	0.31
k	−4.9 ± 0.5		−9.5 ± 0.8		<0.01
$Ca_V2.1$					
$V_{½}$ (mV)	−18 ± 0.8	8	−6.1 ± 2.5	8	<0.01
k	−3.0 ± 0.4		−4.3 ± 0.9		0.27
$Ca_V3.1$					
$V_{½}$ (mV)	−62.5 ± 0.8	7	−60.5 ± 1	7	0.24
k	−3.9 ± 0.1		−3.4 ± 0.1		0.04

Table 3

Parameters for voltage-dependent activation

Values for $V_{½}$ and k were obtained from Boltzmann fits of data in Fig. 5*B*; n represents number of cells. Results were obtained from nine independent experiments and p values were determined by t test.

Channel	WT	*n*	Mutant	*n*	*p* value
$Ca_V1.3$					
$V_{½}$ (mV)	−7.8 ± 1.6	9	−5.6 ± 1.5	10	0.36
k	8 ± 0.9		10.3 ± 0.8		0.10
$Ca_V2.1$					
$V_{½}$ (mV)	8.6 ± 1.6	7	11.8 ± 1.4	8	0.21
k	7.5 ± 0.5		5.7 ± 1		0.24
$Ca_V3.1$					
$V_{½}$ (mV)	−37.1 ± 0.9	7	−32.4 ± 0.9	8	<0.01
k	3.3 ± 0.3		4.7 ± 0.4		0.03

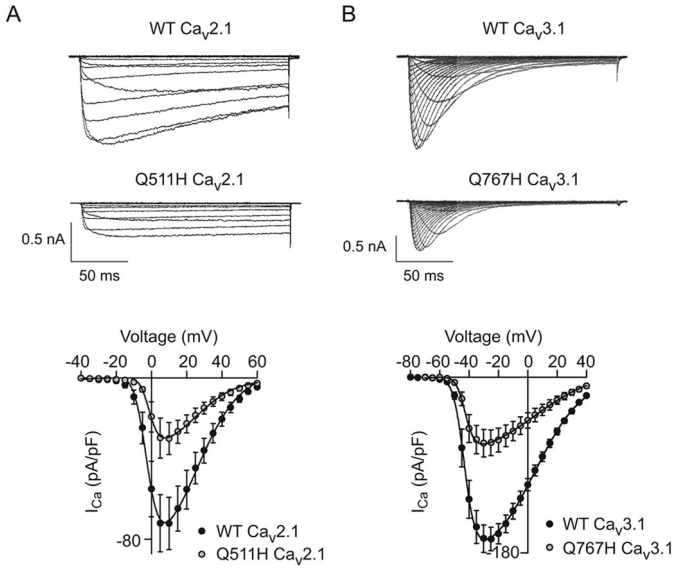

Figure 6. The corresponding mutation of Q511H in $Ca_v2.1$ and Q767H $Ca_v3.1$ suppress current density. *A* and *B*, representative traces (*top*) and I-V relationships (*B*) for WT ($n = 8$ cells) and mutant $Ca_v2.1$ channels ($n = 9$ cells, *A*) or WT ($n = 11$ cells) and mutant $Ca_v3.1$ channels ($n = 14$ cells, *B*). Voltage protocol was the same as in Fig. 2*A*. Results are from four independent experiments. *Error bars* represent S.E.

cant reduction in Q_{max} because of the Gln to His mutations (21.9 ± 1.8 fC for WT $Ca_v2.1$ *versus* 10.2 ± 1.9 fC for Q511H, $p < 0.01$ by t test; 95.1 ± 16.9 fC for WT $Ca_v3.1$ *versus* 26.2 ± 4.6 fC for Q767H, $p < 0.01$ by t test), but no change in the slope of the I_{tail} *versus* Q_{max} relationship (42.9 ± 3.8 for WT $Ca_v2.1$ *versus* 41 ± 5.6 for Q511H, $p = 0.76$ by F-test; 51.5 ± 3.7 for WT $Ca_v3.1$ *versus* 69.3 ± 8.6 for Q767H, $p = 0.45$ by F-test) (Fig. 7). Thus, the Gln to His mutations in all three classes of Ca_v channel decrease the number of functional channels, but not their open probability, which could be explained by decreased levels of channels in the plasma membrane.

Steady-state inactivation was also suppressed by Q511H as compared with WT $Ca_v2.1$, but was more severe than Q558H in $Ca_v1.3$ in that there was a strong positive shift in $V_{½}$ because of Q511H (Fig. 8*A*; Table 2). Although voltage-dependent activation of Q511H was not affected (Fig. 8*B*; Table 3), the window current generated by the mutant channels was greater than for WT channels because of lack of inactivation at positive voltages (Fig. 8*C*). In contrast to the robust effects of Q558H and Q511H on inactivation in $Ca_v1.3$ and $Ca_v2.1$, respectively, VDI of $Ca_v3.1$ was not affected by Q767H (Fig. 9*A*; Table 2). Although

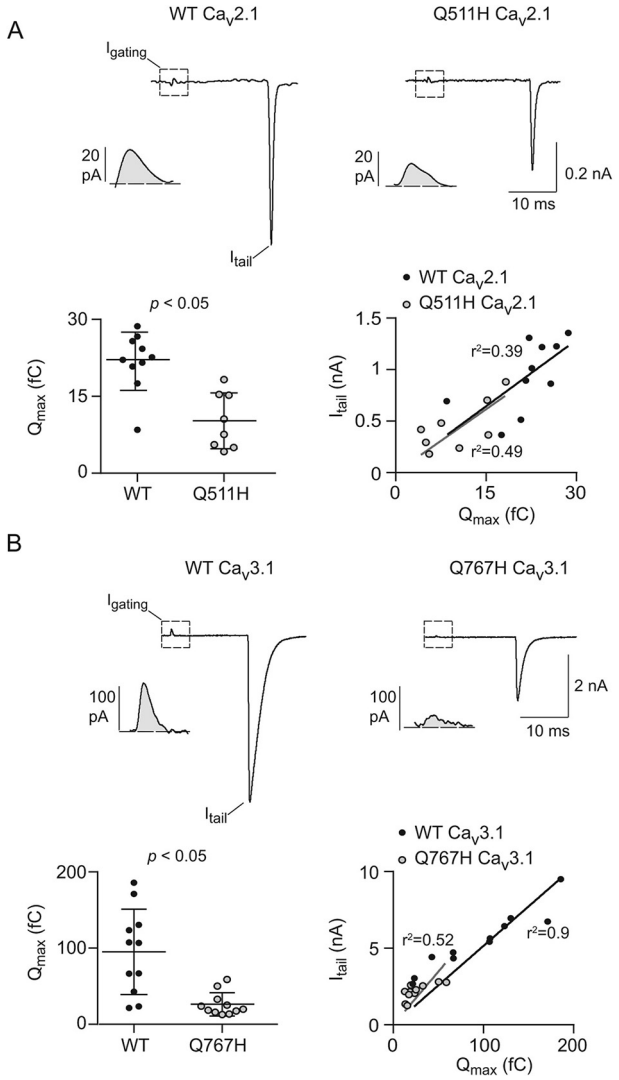

Figure 7. Q511H in $Ca_V2.1$ and Q767H in $Ca_V3.1$ decrease the number of functional channels. *A*, *top*, representative current traces from WT (*left*) or Q511H mutant (*right*) $Ca_V2.1$ channels showing I_{gating} evoked by a 20-ms step depolarization from −80 mV to +70 mV and I_{tail} upon repolarization to −80 mV. *Insets* show I_{gating} on expanded time scale. *Bottom left*, average maximal gating charge (Q_{max}) for WT (n = 10 cells) and Q511H mutant $Ca_V2.1$ channels (n = 8 cells); p value was determined by t test. *Bottom right*, I_{tail} for each cell is plotted against Q_{max}. The fit by linear regression and coefficient of determination (r^2) are shown for WT and mutant channels. Results are from four independent experiments. *Error bars* represent S.E. *B*, same as in *A* except for WT (n = 11 cells) and Q767H mutant $Ca_V3.1$ channels (n = 11 cells). Results are from four independent experiments.

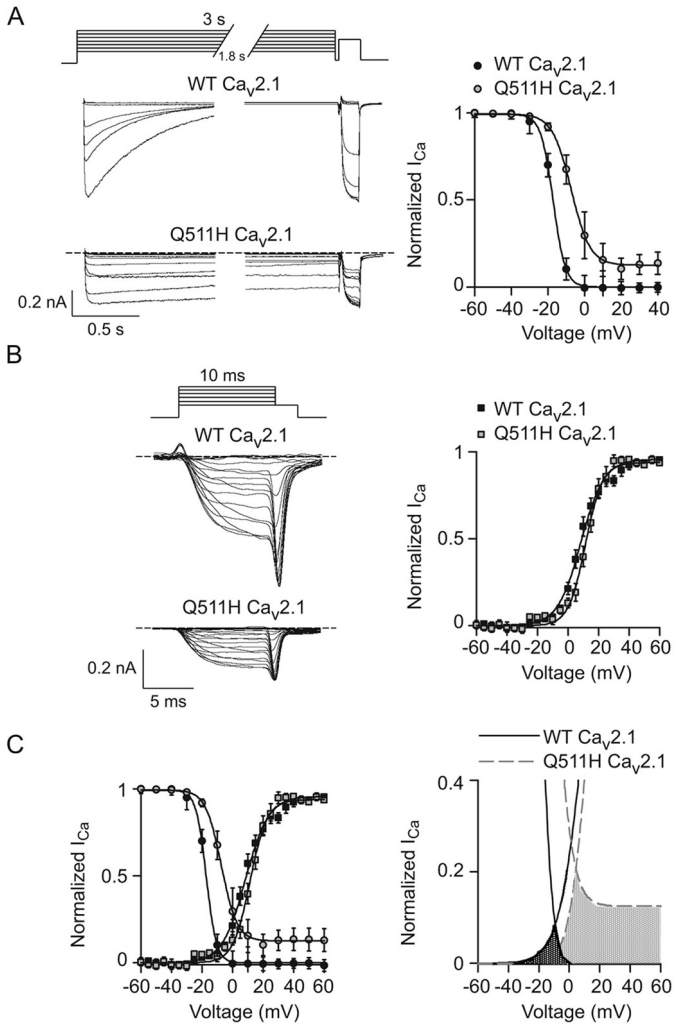

Figure 8. Q511H suppresses voltage-dependent inactivation of $Ca_V2.1$. *A–C*, same as in Fig. 5 except that the inactivation protocol was essayed with 3-s prepulses in cells transfected with WT (n = 15 cells) or Q511H mutant $Ca_V2.1$ channels (n = 16 cells). Results are from six independent experiments. *Error bars* represent S.E.

Q767H modestly suppressed voltage-dependent activation of $Ca_V3.1$ (Fig. 9*B*; Table 3), there was limited impact of this mutation on the window current (Fig. 9*C*). We conclude that Gln-558 and Gln-511 are determinants regulating VDI of high-voltage activated (*i.e.* Ca_V1 and Ca_V2) Ca^{2+} channels, and of the cell-surface density of all Ca_V channel family members.

Discussion

VDI is a crucial feature of most Ca_V channels, limiting Ca^{2+} influx that could otherwise cause aberrant cellular excitability (23, 24). A variety of factors regulate VDI of Ca_V channels, including the auxiliary $Ca_V\beta$ subunit (reviewed in Ref. 25). Within the main α_1 subunit, multiple elements contributing to VDI of Ca_V1 and Ca_V2 channels have been identified in cytoplasmic regions (26–28) or transmembrane segments (29, 30). Considering that Gln-558 and Gln-511 are located in the extracellular S1–S2 loop of domain II (IIS1–S2L) (Fig. 1), how these residues might promote VDI (Figs. 5 and 7) is unclear. Together with S3 and S4, S1 and S2 form the voltage sensor domain (VSD), a conserved module in voltage-gated ion channels that senses changes in the cell membrane potential in ways that alter the opening, closing, and inactivation of the channel (31). Within Ca_V1 and Ca_V2 channels, VSDs in domains I through IV may be functionally heterogeneous, with domains II and III playing the most prominent roles in voltage-dependent activation (32) and VDI (33). Thus, Gln-558 and Gln-511 may modulate the contribution of the VSD in domain II (VSDII) to gating of VDI. In the structure of the skeletal muscle $Ca_V1.1$ complex by cryo-EM, S1–S2 loops are closely associated with the pore-lining S5–S6 loop (34). The substitution of a charged histidine residue at this site might produce electrostatic alterations that destabilize VDI by maintaining the pore in an open rather than inactivated conformation (Figs. 5 and 7). Determinants for VDI

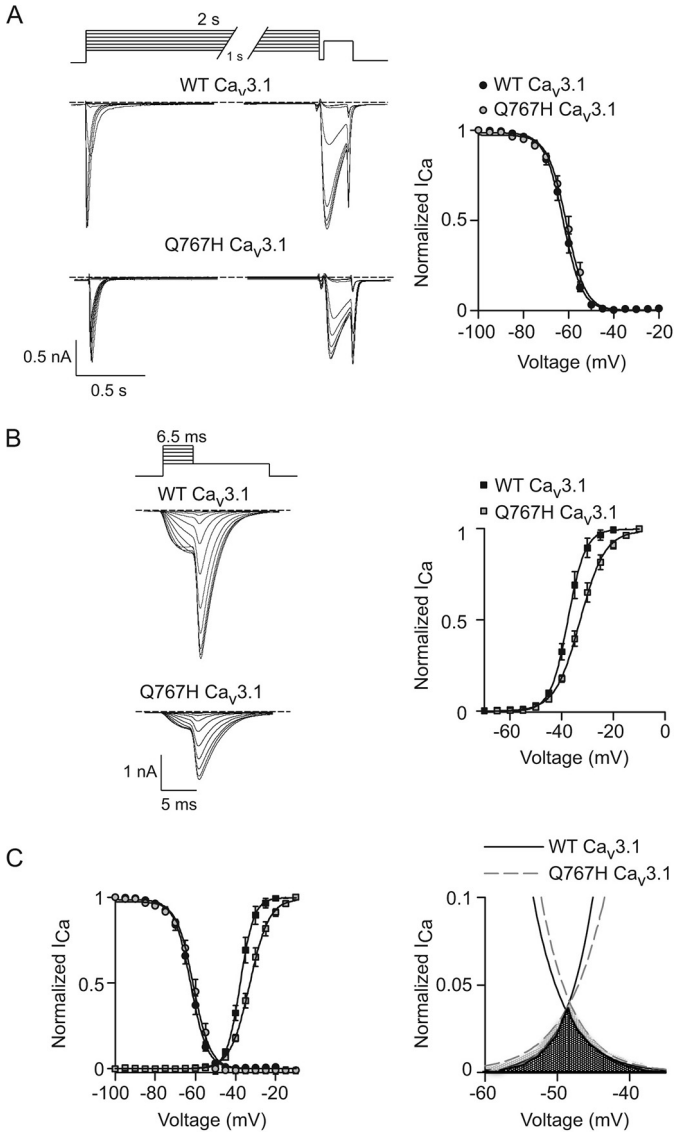

Figure 9. Q767H does not affect voltage-dependent inactivation of $Ca_v3.1$. *A–C*, same as in Fig. 5 except that inactivation protocol was essayed with 2-s prepulses and the tail currents were evoked by 6.5-ms steps to various voltages prior to 30-ms repolarization to −100 mV in cells transfected with WT ($n = 14$ cells) or Q767H mutant $Ca_v3.1$ channels ($n = 15$ cells). Results are from six independent experiments. *Error bars* represent S.E.

in Ca_v3 channels differ from those in Ca_v1 and Ca_v2 channels (35), which may explain the lack of effect of the Gln to His mutation on $Ca_v3.1$ VDI (Fig. 9).

At first glance, the inhibitory effects of the Gln to His mutations on current density in all three classes of Ca_v channels (Figs. 2 and 6) might simply result from a decrease in the stability of the channel protein. However, in the context of $Ca_v1.3$, Q558H diminished the amount of $Ca_v1.3$ protein on the cell surface but had no effect on total protein $Ca_v1.3$ levels (Fig. 3). Moreover, gating current analyses indicate a decrease in the number of functional $Ca_v1.3$ channels with the Q558H mutation (Fig. 2, *B* and *C*). Taken together, these results suggest that the decrease in current density caused by the Gln to His mutation results from an impairment in the trafficking and/or maintenance of channels in the plasma membrane. Although auxiliary $\alpha_2\delta$ subunit promotes the cell-surface trafficking of these channels through interactions with extracellular sites in the α_1 subunit (reviewed in Ref. 36), the Gln to His mutations are unlikely to disrupt the interaction of $Ca_v1.3$ and $Ca_v2.1$ with $\alpha_2\delta$ given that domain II S1–S2 is distant from sites in Ca_v α_1 that are found in contact with $\alpha_2\delta$ based on the cryo-EM structure of $Ca_v1.1$ (34). Moreover, Q767H also significantly reduces the current density of $Ca_v3.1$ expressed without $\alpha_2\delta$ (Fig. 6*B*).

Within K_v channels, a conserved threonine in the S1–S2 linker (S1–S2L) is required for efficient trafficking of the channel to the plasma membrane (37, 38). This residue is thought to interact with a glutamate in the S5–S6L (39), which may stabilize VSDs and gating domains in ways that support K_v channel trafficking out of the endoplasmic reticulum and into the plasma membrane (37). In the cryo-EM structure of $Ca_v1.1$, the S1–S2L in all the VSDs is well resolved, indicative of rigidity that may be important for its interaction with LS5–S6 (34). Similar to the role of S1–S2L in K_v channels (37, 38), efficient trafficking of Ca_v channels may depend on the contact between S1–S2L and S5–S6L, and this is disrupted by the Gln to His mutation.

It is important to note that both the proband and his parents possess a variant in *OTOG*, a gene that is associated with autosomal-recessive moderate hearing impairment (15). Thus we cannot conclude whether it is the *OTOG* and/or *CACNA1D* variant that contributes to the hearing impairment of the affected individual. However, there are 12 reported mutations in *OTOG* of which 11 are lack of function, and only 1 reported missense mutation, making the mutation in this gene less of a candidate for the individual's symptoms. Considering the additional phenotypes of the proband, it is noteworthy that gain of function mutations in *CACNA1D* are associated with autism spectrum disorder (ASD) and epilepsy (7, 8). Like Q567H, these mutations cause an increase in the window current mediated by $Ca_v1.3$. However, the mechanism involves a slowing of VDI and/or enhancement in voltage-dependent activation (7, 8), in contrast to the selective effect of Q558H on suppressing VDI (Figs. 4 and 5). The gain of function in $Ca_v1.3$ would be expected to cause abnormalities in the morphology of dendritic spines (40), which have been linked to ASD (41) and epilepsy (42). $Ca_v1.3$ regulates neuronal excitability and synaptic plasticity in the striatum (43–46), a brain region implicated in the neuropathology of ASD (47). However, we are cautious in noting that the impact of Q558H on $Ca_v1.3$ properties may be influenced by additional factors present in neurons that are absent from HEK293T cells. As has been demonstrated for ASD-linked mutations in $Ca_v1.2$ (48–50), an understanding of how these gain of function mutations in $Ca_v1.3$ contribute neurodevelopmental and neurological disorders will be facilitated by the development of appropriate animal models.

Experimental procedures

Genetic analysis

This study abides by the Declaration of Helsinki principles and was approved by the Institutional Review Board at Hadassah-Hebrew University Hospital. Affected patients' guardians gave informed consent for exome sequencing and to publication of this study.

Whole exome sequencing was performed as described previously (51). Briefly, exonic sequences were enriched using SureSelect Human All Exon 50 megabase kit (Agilent Technologies, Santa Clara, CA). Sequences were determined by HiSeq 2500 (Illumina, San Diego, CA) as 100-bp paired-end runs. Data analysis including read alignment and variant calling was performed by DNAnexus software (Palo Alto, CA) using the default parameters with the human genome assembly hg19 (GRCh37) as reference. Exome analysis of the analyzed individuals yielded 44.1 million mapped reads with a coverage of 86.0×. Following alignment to the reference genome (hg19) and variant calling, variants were filtered out if they were off-target (>8 bp from splice junction), synonymous (>3 bp from splice junction), or had minor allele frequency >0.01 in the ExAC database (Exome Aggregation Consortium, Cambridge, MA; URL: http://exac.broadinstitute.org)[3] or in our in-house exome database comprising ~2500 exomes. All potentially causative variants were confirmed using Sanger sequencing.

Molecular biology

The following cDNAs were used: $Ca_V1.3$ (GenBank™ no. AF370009), $Ca_V2.1$ (GenBank™ no. NM_001127221), $Ca_v3.1$ (AF190860), β_{2a} (GenBank™ no. NC013684), and $\alpha_2\delta_1$ (GenBank™ no. M76559.1). The Q558H mutation was inserted into the corresponding regions of the domain II S1–S2 linker (IIS1–S2L) in $Ca_V1.3$, $Ca_V2.1$, and $Ca_V3.1$ using the NEBuilder HiFi DNA Assembly cloning system (New England Biolabs). Channel fragments were amplified by PCR with appropriate primers and ligated into the parent plasmid ($Ca_V1.3$/pcDNA6, $Ca_V2.1$/pcDNA3.1, $Ca_V3.1$/pDsRed Express-N1). For the FLAG-tagged $Ca_V1.3$ WT and Q567H constructs, a FLAG epitope with spacer sequences (TRH-DYKDDDDK-VTFDEMQT) was added to the extracellular loop just C-terminal to residue Gly-693 by PCR using NEBuilder HiFi DNA Assembly cloning system (New England Biolabs). The vector was linearized by digestion with BsiWI and BamHI enzymes (New England Biolabs). The entire open reading frames of all the plasmids were verified by sequencing to confirm the presence of the mutation.

Cell culture and transfection

Human embryonic kidney cells transformed with SV40 T-antigen (ATCC, cat. no. CRL-3216, RRID: CVCL_0063) were maintained in Dulbecco's modified Eagle medium (Gibco, 11965) supplemented with 10% fetal bovine serum (Atlanta Biologicals, S11150), at 37 °C in 5% CO_2–95% air humidified atmosphere. For electrophysiological recordings, the cells were grown at ~70% confluent in 35-mm Petri dish prior to transient transfection with Ca_v channel cDNAs using FuGene 6 transfection reagent (Promega, E2691). The following amounts of cDNAs were used: WT or mutant $Ca_V1.3$ or $Ca_V2.1$ (2.5 μg) and 1 μg each of the auxiliary subunits β_{2a} and $\alpha_2\delta_1$. $Ca_v3.1$ (2.5 μg) was transfected without auxiliary subunit cDNAs. In all cases, cDNA encoding the GFP (pEGFP) was cotransfected to aid fluorescent detection of transfected cells. cDNA was incubated with 6 μl of FuGene transfection reagent in 100 μl of FBS-free DMEM in a sterile microfuge tube (1.5 ml). The transfection solution was added to the dish and cells were maintained at 37 °C for 48 h. Two h before its electrophysiological recording the cells were dissociated using Versene reagent (Thermo Fisher Scientific, 15040066) in 35-mm Petri dishes with fresh medium at low density ~20%.

For cell-surface biotinylation assays, HEK293T cells were transfected using Lipofectamine 3000 reagent (Life Technologies, L3000-008) following the manufacturer's protocol. Plasmid DNA (WT or mutant $Ca_v1.3$ (1.2 μg); β_{2a} and $\alpha_2\delta_1$ (0.4 μg each)) was diluted in Opti-MEM (50 μl, Life Technologies) and 4 μl of P3000 Reagent, and added to a mixture of Opti-MEM (50 μl) and Lipofectamine 3000 Reagent (3 μl) and allowed to incubate for 10 min at room temperature. The solution was then added to the cells. The cell culture media were changed after 24 h and cell-surface biotinylation assays were performed 48 h after transfection.

Electrophysiology

Transfected HEK293T cells were recorded with the whole-cell patch clamp technique at room temperature (21–24 °C) using an EPC-8 patch clamp amplifier and Patchmaster software (HEKA Elektronik). Electrophysiological data were sampled at 20 kHz and filtered at 5 kHz. Leak current was subtracted using an online P/4 protocol. The external solution contained the following (in mM): $CaCl_2$ 10, TEA-Cl 125, HEPES 10, and glucose 10, pH 7.3, with TEA-OH. The internal solution contained (in mM): CsCl 110, $MgCl_2$ 5, EGTA 10, HEPES 10, Na-ATP 4, GTP 0.1, pH 7.3, with CsOH. The recording pipettes had a resistance in the bath solution in the range of 4–7 megohms. All reagents were purchased from Sigma-Aldrich.

Current-voltage relationships were obtained from the peak amplitude of currents evoked by 200-ms depolarizations from −80 mV to various voltages in 5-mV increments. I-V data were fit with the Boltzmann equation: $I = G\cdot(V - E)/(1 + \exp(-(V - V_{½})/k))$, where G is conductance, E is the reversal potential, $V_{½}$ is the voltage of half-maximal activation, and k is the slope factor for activation. The current density was obtained by normalizing the current amplitude with the membrane capacitance.

The kinetics of inactivation were measured by fitting traces of currents with a double exponential function: $I = A_{fast}\exp(-t/\tau_{fast}) + F_{slow}\exp(-t/\tau_{slow})$, where t is time, and A_{fast} and A_{slow} are the amplitudes of the current decaying with corresponding time constants (τ). The fraction of the total inactivating current ($A_{fast} + A_{slow}$) corresponding to fast inactivation was determined as $F_{fast} = A_{fast}/(A_{fast} + A_{slow})$ and that for slow inactivation (F_{slow}) was determined as $A_{slow}/(A_{fast} + A_{slow})$.

For measuring steady-state inactivation, a conditioning prepulse to various voltages preceded a test depolarization to +10 mV for $Ca_V1.3$ and $Ca_V2.1$ and to −30 mV for $Ca_V3.1$. Inactivation curves were fitted with the Boltzmann function: $I = I_{max}/(1 + \exp(V - V_{½})/k)$, where I represents test current amplitude, V is test voltage, $V_{½}$ is the voltage of half-maximal inactivation, and k is the slope factor. Voltage dependence of activation was measured by plotting the normalized tail currents evoked by 2-ms repolarizations to −60 mV from 10-ms pulses to vari-

[3] Please note that the JBC is not responsible for the long-term archiving and maintenance of this site or any other third party hosted site.

ous voltages, followed by fitting with the above Boltzmann function.

Data were analyzed using custom routines in Igor Pro software (WaveMetrics) and SigmaPlot (Systat Software Inc., San Jose, CA). Averaged data are shown as the mean ± S.E. For statistical analysis, data were first analyzed for normality by Shapiro-Wilk test followed by Student's *t* test with differences considered statically significant when $p < 0.05$. For gating current analysis, the data were fit by linear regression and the slopes compared by F-test.

Biochemical analysis of cell-surface $Ca_v1.3$ protein

HEK293T cells were transfected with WT and mutant $Ca_v1.3$ and auxiliary subunits as described above, and 1 day later, cell-surface proteins were labeled with a biotin labeling kit (Thermo Scientific, cat. no.89881) according to the manufacturer's protocol. Briefly, transfected cells were quickly washed with ice-cold phosphate buffered saline containing the following (in mM): 2.5 KCl, 136 NaCl, 1.5 KH_2PO_4, 6.5 Na_2HPO_4 (pH 7.4), and incubated with 0.25 mg/ml of the cell membrane impermeable biotinylation reagent sulfo-NHS-SS-biotin for 30 min at 4 °C. To stop the reaction, the cells were then incubated with biotin quenching solution containing (in mM): glycine 50, $CaCl_2$ 2.5, $MgCl_2$ 1, pH 7.4. The cells were pelleted by centrifugation and resuspended in radioimmune precipitation assay buffer containing (in mM) NaCl 150, PMSF 0.5, Tris-HCl 25, pH 7.6, with 1% Nonidet P-40, 1% Na deoxycholate, 0.1% SDS, and protease inhibitors. After 10 min incubation on ice, cell lysates were subject to centrifugation (16,000 × *g* for 10 min at 4 °C) and biotinylated proteins recovered with NeutrAvidin gel. The bound proteins were eluted by incubating with SDS-PAGE sample buffer (58 mM Tris-Cl, 50 mM DTT, 1.7% SDS, 5% glycerol, 0.002% bromphenol blue, pH 6.8, and subject to electrophoresis using Novex™ WedgeWell™ 4–20% Tris-Glycine gel (Invitrogen cat. no.105955) and transfer to nitrocellulose blotting membranes (Amersham Biosciences, Protran 0.2 μm NC, cat. no. 10600001).

For Western blotting, the membranes were incubated in blocking buffer containing milk (5%) in TBS-T (100 mM Tris-HCl, 0.15 M NaCl, 0.05% Tween 20) followed by incubation with the following antibodies diluted in blocking buffer: $Ca_V1.3$ (1:3000) (52), N^+/K^+ ATPase (1:700) (Developmental Studies Hybridoma Bank at University of Iowa, cat. no. a6F RRID: AB_2314847), and GAPDH (1:10,000) (Cell Signaling Technology, cat. no. 14C10). Secondary antibodies used were anti-rabbit HRP (1:3000) (GE Healthcare, cat. no. NA934–1ML), and anti-mouse HRP (1:3000) (GE Healthcare, cat. no. NA931V) followed by chemiluminescent detection (Thermo Scientific, SuperSignal West Pico cat. no. 34080). The Western blotting signals were visualized with the Odyssey Fc Imaging System (LI-COR). The results shown were obtained from at least three independent experiments. Densitometric analysis was performed with Image Studio Lite software (LI-COR).

Double-label immunofluorescence

HEK293T cells were transfected as described for cell-surface biotinylation experiments except that FLAG-tagged $Ca_v1.3$ and Q567H cDNAs were used, and cells were plated on glass coverslips. Sequential double-labeling for cell-surface and total channels was performed as described previously (53). Twenty-four h post transfection, the cells were rinsed in PBS and incubated with mouse anti-FLAG M2 antibody (Sigma-Aldrich) (1:50 diluted in DMEM media with 10% FBS) at room temperature for 30 min. The cells were then rinsed in PBS and fixed with 4% paraformaldehyde in PBS. After rinsing three times with PBS the cells were then blocked using 5% normal goat serum and 0.3% Triton X-100 in PBS for 30 min at room temperature and incubated with rabbit anti $Ca_v1.3$ antibodies to label the total intracellular and cell-surface channels for 1 h at room temperature. After three times with PBS, cells were incubated in secondary antibodies (RhoRed-X 568 anti-rabbit and Alexa Fluor 488 anti-mouse, Jackson ImmunoResearch Laboratories) (1:1000 each diluted in 5% normal goat serum and 0.1% Triton X-100 in PBS) for 1 h at room temperature. Coverslips were rinsed again three times in PBS and one time with water before mounting in Fluoromount G (Electron Microscopy Sciences, 17984–25). Labeled cells were visualized with a 60× oil-immersion objective on a confocal microscope (Fluoview 1000, Olympus). Images were acquired at 510 for 488 channel and 500 for 568 channel laser intensity and processed in ImageJ.

Author contributions—E. G.-L. and A. L. formal analysis; E. G.-L., J. A. L., J. H., R. S., V. M., and A. L. investigation; E. G.-L., R. S., V. M., and A. L. writing-review and editing; V. M. and A. L. conceptualization; V. M. and A. L. resources; V. M. and A. L. supervision; V. M. and A. L. project administration; A. L. funding acquisition; A. L. writing-original draft.

Acknowledgments—We thank Dr. Jianping Wu for helpful insights, and Mackenzie McKnight and Brian Goodell for excellent technical assistance.

References

1. Hübner, C. A., and Jentsch, T. J. (2002) Ion channel diseases. *Hum. Mol. Genet.* **11,** 2435–2445 CrossRef Medline
2. Grant, A. O., Carboni, M. P., Neplioueva, V., Starmer, C. F., Memmi, M., Napolitano, C., and Priori, S. (2002) Long QT syndrome, Brugada syndrome, and conduction system disease are linked to a single sodium channel mutation. *J. Clin. Invest.* **110,** 1201–1209 CrossRef Medline
3. Wehrens, X. H., Rossenbacker, T., Jongbloed, R. J., Gewillig, M., Heidbuchel, H., Doevendans, P. A., Vos, M. A., Wellens, H. J., and Kass, R. S. (2003) A novel mutation L619F in the cardiac Na^+ channel SCN5A associated with long-QT syndrome (LQT3): A role for the I–II linker in inactivation gating. *Hum. Mutat.* **21,** 552 CrossRef Medline
4. Singh, A., Hamedinger, D., Hoda, J. C., Gebhart, M., Koschak, A., Romanin, C., and Striessnig, J. (2006) C-terminal modulator controls Ca^{2+}-dependent gating of $Ca_v1.4$ L-type Ca^{2+} channels. *Nat. Neurosci.* **9,** 1108–1116 CrossRef Medline
5. Pietrobon, D. (2010) CaV2.1 channelopathies. *Pflugers Arch.* **460,** 375–393 CrossRef Medline
6. Striessnig, J., Bolz, H. J., and Koschak, A. (2010) Channelopathies in Cav1.1, Cav1.3, and Cav1.4 voltage-gated L-type Ca^{2+} channels. *Pflugers Arch.* **460,** 361–374 CrossRef Medline
7. Pinggera, A., Lieb, A., Benedetti, B., Lampert, M., Monteleone, S., Liedl, K. R., Tuluc, P., and Striessnig, J. (2015) *CACNA1D* de novo mutations in autism spectrum disorders activate Cav1.3 L-type calcium channels. *Biol. Psychiatry* **77,** 816–822 CrossRef Medline
8. Pinggera, A., Mackenroth, L., Rump, A., Schallner, J., Beleggia, F., Wollnik, B., and Striessnig, J. (2017) New gain-of-function mutation shows

CACNA1D as recurrently mutated gene in autism spectrum disorders and epilepsy. *Hum. Mol. Genet.* **26,** 2923–2932 CrossRef Medline

9. Platzer, J., Engel, J., Schrott-Fischer, A., Stephan, K., Bova, S., Chen, H., Zheng, H., and Striessnig, J. (2000) Congenital deafness and sinoatrial node dysfunction in mice lacking class D L-type Ca^{2+} channels. *Cell* **102,** 89–97 CrossRef Medline
10. Brandt, A., Striessnig, J., and Moser, T. (2003) $Ca_V1.3$ channels are essential for development and presynaptic activity of cochlear inner hair cells. *J. Neurosci.* **23,** 10832–10840 CrossRef Medline
11. Baig, S. M., Koschak, A., Lieb, A., Gebhart, M., Dafinger, C., Nürnberg, G., Ali, A., Ahmad, I., Sinnegger-Brauns, M. J., Brandt, N., Engel, J., Mangoni, M. E., Farooq, M., Khan, H. U., Nürnberg, P., Striessnig, J., and Bolz, H. J. (2011) Loss of $Ca_v1.3$ (*CACNA1D*) function in a human channelopathy with bradycardia and congenital deafness. *Nat. Neurosci.* **14,** 77–84 CrossRef Medline
12. Sinnegger-Brauns, M. J., Huber, I. G., Koschak, A., Wild, C., Obermair, G. J., Einzinger, U., Hoda, J. C., Sartori, S. B., and Striessnig, J. (2009) Expression and 1,4-dihydropyridine-binding properties of brain L-type calcium channel isoforms. *Mol. Pharmacol.* **75,** 407–414 CrossRef Medline
13. McKinney, B. C., and Murphy, G. G. (2006) The L-type voltage-gated calcium channel $Ca_V1.3$ mediates consolidation, but not extinction, of contextually conditioned fear in mice. *Learn. Mem.* **13,** 584–589 CrossRef Medline
14. Simmler, M. C., Cohen-Salmon, M., El-Amraoui, A., Guillaud, L., Benichou, J. C., Petit, C., and Panthier, J. J. (2000) Targeted disruption of *Otog* results in deafness and severe imbalance. *Nat. Genet.* **24,** 139–143 CrossRef Medline
15. Schraders, M., Ruiz-Palmero, L., Kalay, E., Oostrik, J., del Castillo, F. J., Sezgin, O., Beynon, A. J., Strom, T. M., Pennings, R. J., Zazo Seco, C., Oonk, A. M., Kunst, H. P., Domínguez-Ruiz, M., García-Arumi, A. M., del Campo, M., *et al.* (2012) Mutations of the gene encoding otogelin are a cause of autosomal-recessive nonsyndromic moderate hearing impairment. *Am. J. Hum. Genet.* **91,** 883–889 CrossRef Medline
16. Dou, H., Vazquez, A. E., Namkung, Y., Chu, H., Cardell, E. L., Nie, L., Parson, S., Shin, H. S., and Yamoah, E. N. (2004) Null mutation of α_{1D} Ca^{2+} channel gene results in deafness but no vestibular defect in mice. *J. Assoc. Res. Otolaryngol.* **5,** 215–226 CrossRef Medline
17. Scholl, U. I., Goh, G., Stölting, G., de Oliveira, R. C., Choi, M., Overton, J. D., Fonseca, A. L., Korah, R., Starker, L. F., Kunstman, J. W., Prasad, M. L., Hartung, E. A., Mauras, N., Benson, M. R., Brady, T., *et al.* (2013) Somatic and germline *CACNA1D* calcium channel mutations in aldosterone-producing adenomas and primary aldosteronism. *Nat. Genet.* **45,** 1050–1054 CrossRef Medline
18. Klassen, T., Davis, C., Goldman, A., Burgess, D., Chen, T., Wheeler, D., McPherson, J., Bourquin, T., Lewis, L., Villasana, D., Morgan, M., Muzny, D., Gibbs, R., and Noebels, J. (2011) Exome sequencing of ion channel genes reveals complex profiles confounding personal risk assessment in epilepsy. *Cell* **145,** 1036–1048 CrossRef Medline
19. Takahashi, S. X., Miriyala, J., and Colecraft, H. M. (2004) Membrane-associated guanylate kinase-like properties of β-subunits required for modulation of voltage-dependent Ca^{2+} channels. *Proc. Natl. Acad. Sci. U.S.A.* **101,** 7193–7198 CrossRef Medline
20. Wei, X., Neely, A., Lacerda, A. E., Olcese, R., Stefani, E., Perez-Reyes, E., and Birnbaumer, L. (1994) Modification of Ca^{2+} channel activity by deletions at the carboxyl terminus of the cardiac α_1 subunit. *J. Biol. Chem.* **269,** 1635–1640 Medline
21. Altier, C., Dubel, S. J., Barrère, C., Jarvis, S. E., Stotz, S. C., Spaetgens, R. L., Scott, J. D., Cornet, V., De Waard, M., Zamponi, G. W., Nargeot, J., and Bourinet, E. (2002) Trafficking of L-type calcium channels mediated by the postsynaptic scaffolding protein AKAP79. *J. Biol. Chem.* **277,** 33598–33603 CrossRef Medline
22. Christel, C., and Lee, A. (2012) Ca^{2+}-dependent modulation of voltage-gated Ca^{2+} channels. *Biochim. Biophys. Acta* **1820,** 1243–1252 CrossRef Medline
23. Hennessey, J. A., Boczek, N. J., Jiang, Y. H., Miller, J. D., Patrick, W., Pfeiffer, R., Sutphin, B. S., Tester, D. J., Barajas-Martinez, H., Ackerman, M. J., Antzelevitch, C., Kanter, R., and Pitt, G. S. (2014) A *CACNA1C* variant associated with reduced voltage-dependent inactivation, increased $Ca_V1.2$ channel window current, and arrhythmogenesis. *PLoS One* **9,** e106982 CrossRef Medline
24. Barrett, C. F., and Tsien, R. W. (2008) The Timothy syndrome mutation differentially affects voltage- and calcium-dependent inactivation of $Ca_V1.2$ L-type calcium channels. *Proc. Natl. Acad. Sci. U.S.A.* **105,** 2157–2162 CrossRef Medline
25. Buraei, Z., and Yang, J. (2013) Structure and function of the β subunit of voltage-gated Ca^{2+} channels. *Biochim. Biophys. Acta* **1828,** 1530–1540 CrossRef Medline
26. Herlitze, S., Hockerman, G. H., Scheuer, T., and Catterall, W. A. (1997) Molecular determinants of inactivation and G protein modulation in the intracellular loop connecting domains I and II of the calcium channel α1A subunit. *Proc. Natl. Acad. Sci. U.S.A.* **94,**1512–1516 Medline
27. Berrou, L., Bernatchez, G., and Parent, L. (2001) Molecular determinants of inactivation within the I–II linker of α1E ($Ca_V2.3$) calcium channels. *Biophys. J.* **80,** 215–228 CrossRef Medline
28. Bourinet, E., Soong, T. W., Sutton, K., Slaymaker, S., Mathews, E., Monteil, A., Zamponi, G. W., Nargeot, J., and Snutch, T. P. (1999) Splicing of α_{1A} subunit gene generates phenotypic variants of P- and Q-type calcium channels. *Nat. Neurosci.* **2,** 407–415 CrossRef Medline
29. Stotz, S. C., and Zamponi, G. W. (2001) Identification of inactivation determinants in the domain IIS6 region of high voltage-activated calcium channels. *J. Biol. Chem.* **276,** 33001–33010 CrossRef Medline
30. Tadross, M. R., Ben Johny, M., and Yue, D. T. (2010) Molecular endpoints of Ca^{2+}/calmodulin- and voltage-dependent inactivation of $Ca_V1.3$ channels. *J. Gen. Physiol.* **135,** 197–215 CrossRef Medline
31. Palovcak, E., Delemotte, L., Klein, M. L., and Carnevale, V. (2014) Evolutionary imprint of activation: The design principles of VSDs. *J. Gen. Physiol.* **143,** 145–156 CrossRef Medline
32. Pantazis, A., Savalli, N., Sigg, D., Neely, A., and Olcese, R. (2014) Functional heterogeneity of the four voltage sensors of a human L-type calcium channel. *Proc. Natl. Acad. Sci. U.S.A.* **111,** 18381–18386 CrossRef Medline
33. Spaetgens, R. L., and Zamponi, G. W. (1999) Multiple structural domains contribute to voltage-dependent inactivation of rat brain α_{1E} calcium channels. *J. Biol. Chem.* **274,** 22428–22436 CrossRef Medline
34. Wu, J., Yan, Z., Li, Z., Qian, X., Lu, S., Dong, M., Zhou, Q., and Yan, N. (2016) Structure of the voltage-gated calcium channel $Ca_V1.1$ at 3.6 Å resolution. *Nature* **537,** 191–196 CrossRef Medline
35. Hamid, J., Peloquin, J. B., Monteil, A., and Zamponi, G. W. (2006) Determinants of the differential gating properties of $Ca_V3.1$ and $Ca_V3.3$ T-type channels: A role of domain IV? *Neuroscience* **143,** 717–728 CrossRef Medline
36. Dolphin, A. C. (2013) The $\alpha2\delta$ subunits of voltage-gated calcium channels. *Biochim. Biophys. Acta* **1828,** 1541–1549 CrossRef Medline
37. McKeown, L., Burnham, M. P., Hodson, C., and Jones, O. T. (2008) Identification of an evolutionarily conserved extracellular threonine residue critical for surface expression and its potential coupling of adjacent voltage-sensing and gating domains in voltage-gated potassium channels. *J. Biol. Chem.* **283,** 30421–30432 CrossRef Medline
38. Füll, Y., Seebohm, G., Lerche, H., and Maljevic, S. (2013) A conserved threonine in the S1–S2 loop of $K_V7.2$ and $K_V7.3$ channels regulates voltage-dependent activation. *Pflugers Arch.* **465,** 797–804 CrossRef Medline
39. Long, S. B., Campbell, E. B., and Mackinnon, R. (2005) Voltage sensor of $K_V1.2$: structural basis of electromechanical coupling. *Science* **309,** 903–908 CrossRef Medline
40. Stanika, R., Campiglio, M., Pinggera, A., Lee, A., Striessnig, J., Flucher, B. E., and Obermair, G. J. (2016) Splice variants of the $Ca_V1.3$ L-type calcium channel regulate dendritic spine morphology. *Sci. Rep.* **6,** 34528 CrossRef Medline
41. Joensuu, M., Lanoue, V., and Hotulainen, P. (2018) Dendritic spine actin cytoskeleton in autism spectrum disorder. *Prog. Neuropsychopharmacol. Biol. Psychiatry* **84,** 362–381 CrossRef Medline
42. Stawarski, M., Stefaniuk, M., and Wlodarczyk, J. (2014) Matrix metalloproteinase-9 involvement in the structural plasticity of dendritic spines. *Front. Neuroanat.* **8,** 68 CrossRef Medline
43. Olson, P. A., Tkatch, T., Hernandez-Lopez, S., Ulrich, S., Ilijic, E., Mugnaini, E., Zhang, H., Bezprozvanny, I., and Surmeier, D. J. (2005) G-pro-

tein-coupled receptor modulation of striatal $Ca_V1.3$ L-type Ca^{2+} channels is dependent on a Shank-binding domain. *J. Neurosci.* **25,** 1050–1062 CrossRef Medline

44. Zhang, H., Fu, Y., Altier, C., Platzer, J., Surmeier, D. J., and Bezprozvanny, I. (2006) $Ca_V1.2$ and $Ca_V1.3$ neuronal L-type calcium channels: Differential targeting and signaling to pCREB. *Eur. J. Neurosci.* **23,** 2297–2310 CrossRef Medline
45. Wang, Z., Kai, L., Day, M., Ronesi, J., Yin, H. H., Ding, J., Tkatch, T., Lovinger, D. M., and Surmeier, D. J. (2006) Dopaminergic control of corticostriatal long-term synaptic depression in medium spiny neurons is mediated by cholinergic interneurons. *Neuron* **50,** 443–452 CrossRef Medline
46. Day, M., Wang, Z., Ding, J., An, X., Ingham, C. A., Shering, A. F., Wokosin, D., Ilijic, E., Sun, Z., Sampson, A. R., Mugnaini, E., Deutch, A. Y., Sesack, S. R., Arbuthnott, G. W., and Surmeier, D. J. (2006) Selective elimination of glutamatergic synapses on striatopallidal neurons in Parkinson disease models. *Nat. Neurosci.* **9,** 251–259 CrossRef Medline
47. Graybiel, A. M. (2016) The striatum and decision-making based on value. in *Micro-, Meso- and Macro-Dynamics of the Brain* (Buzsaki, G., and Christen, Y., eds) pp. 81–84, Springer, New York, NY CrossRef
48. Krey, J. F., Paca, S. P., Shcheglovitov, A., Yazawa, M., Schwemberger, R., Rasmusson, R., and Dolmetsch, R. E. (2013) Timothy syndrome is associated with activity-dependent dendritic retraction in rodent and human neurons. *Nat. Neurosci.* **16,** 201–209 CrossRef Medline
49. Ehlinger, D. G., and Commons, K. G. (2017) Altered $Ca_V1.2$ function in the Timothy syndrome mouse model produces ascending serotonergic abnormalities. *Eur. J. Neurosci.* **46,** 2416–2425 CrossRef Medline
50. Bett, G. C., Lis, A., Wersinger, S. R., Baizer, J. S., Duffey, M. E., and Rasmusson, R. L. (2012) A mouse model of Timothy syndrome: A complex autistic disorder resulting from a point mutation in $Ca_V1.2$. *N. Am. J. Med. Sci.* **5,** 135–140 Medline
51. Harel, T., Hacohen, N., Shaag, A., Gomori, M., Singer, A., Elpeleg, O., and Meiner, V. (2017) Homozygous null variant in CRADD, encoding an adaptor protein that mediates apoptosis, is associated with lissencephaly. *Am. J. Med. Genet.* **173,** 2539–2544 CrossRef Medline
52. Gregory, F. D., Pangrsic, T., Calin-Jageman, I. E., Moser, T., and Lee, A. (2013) Harmonin enhances voltage-dependent facilitation of $Ca_V1.3$ channels and synchronous exocytosis in mouse inner hair cells. *J. Physiol.* **591,** 3253–3269 CrossRef Medline
53. Wang, S., Stanika, R. I., Wang, X., Hagen, J., Kennedy, M. B., Obermair, G. J., Colbran, R. J., and Lee, A. (2017) Densin-180 controls the trafficking and signaling of L-type voltage-gated $Ca_V1.2$ Ca^{2+} channels at excitatory synapses. *J. Neurosci.* **37,** 4679–4691 CrossRef Medline